A finite element method for the contraction analysis of the cardiac tissue: effect of the extracellular collagen network on the myocardial contraction

C. Bourdarias and S. Gerbi [*], J. Ohayon [†]

Abstract

Recent studies in mammalian hearts show that left ventricular wall thickening is an important mechanism for systolic ejection and that during contraction the cardiac muscle develops significant stresses in the muscular cross-fiber direction. We suggested that the collagen network surrounding the muscular fibers could account for these mechanical behaviors. To test this hypothesis we develop a finite element model for large deformation response of active, incompressible, nonlinear elastic and transversely isotropic cardiac tissue in which we include a coupling effect between the connective tissue and the muscular fibers. Then, the three-dimensional finite element formulation including this internal pseudo-active kinematic constraint is written and applied to obtain solutions to an active contraction, uniaxial and equibiaxial extensions of a rectangular sample assuming negligible body forces and inertia. This model could explain the effect of the extracellular collagen network on the myocardial contraction, and the results obtained shown that the proposed connective tissue organization may contribute to the systolic wall thickening.

1 Introduction

Indirect evidence indicates that the characteristics of the passive extracellular connective tissue in the cardiac muscle (myocardium) is an important determinant of ventricular function [16, 14]. Transverse shear along myocardial cleavage planes provides a mechanism for a normal systolic wall thickening. An appropriate constitutive law for myocardium should therefore incorporate the most important features of its microstructure. A sound theoretical formulation for material laws of active myocardium is essential for an accurate mechanical analysis of the stresses in the ventricular wall during the whole cardiac cycle. The wall stress distribution is one of the main factors governing the myocardial energetic ([24]), the coronary blood flow ([15, 5], the cardiac hypertrophy ([1, 9]) and the fetal heart growth ([27, 19]). To date we do not have any reliable technique to evaluate the stress in the cardiac muscle, therefore, mechanical models are useful in cardiology to assess the functional capacities of the human heart. Several numerical models using a finite element (FE) analysis have been done to simulate the left ventricle at end-diastolic state ([11, 12, 13, 10, 6, 7]), and during active myocardial contraction ([3, 12, 17]). Up to now, the mechanical behavior of the

[*]LAMA, Université de Savoie, 73376 Le Bourget du Lac, France. Email: bourdarias@univ-savoie.fr
[†]Laboratoire TIMC, Equipe DynaCell, Domaine de la Merci, 38076 Grenoble Cedex 9, France

connective tissue is assumed isotropic. However, this last assumption is not in agreement with some recent experimental works done on a sample of active myocardial rabbit tissue in which the orientation of the muscle fibers was approximately uniform. Lin and Yin ([16]) shown that, during an active equibiaxial stretch test, there are significant stresses developed in the cross-fiber direction (more than 40% of those in the fiber direction) that cannot be attributed to nonparallel muscle fibers.
Therefore, the purposes of this paper are to: (i) suggest a realistic pseudo-active kinematic law coupling the passive connective tissue to the muscle fibers, which may explain a part of the developed tension in the cross-fiber direction observed by Lin and Yin ([16]), (ii) formulate an active three-dimensional material law for a nonlinear hyperelastic and incompressible continuum medium, which takes care of these coupling effects, (iii) derive the related hree-dimensional finite element (FE), and (iv) test the accuracy and convergence of the proposed numerical methods.

2 Microstructure of the cardiac tissue

2.1 Muscle fiber organization

Anatomical observations have shown that the cardiac muscle tissue has a highly specialized architecture [25]. This structure is composed primarily of cardiac muscle cells, or myocytes that are 80 to 100 μm in length and are roughly cylindrical with cross-sectional dimensions of 10 to 20 μm. These cells are arranged in a more or less parallel weave that we idealize as "muscle fibers". We shall denote the local direction of this group of cells by the unit vector $\mathbf{f}$ and refer to it also as the local "fiber" direction with the understanding that individual continuous muscle fibers do not really exist. Experimental measurements have shown that the muscle fiber direction field defines paths on a nested family or toroidal surfaces of revolution in the wall of the heart [25]. These results show a continuously changing orientation $\mathbf{f}$ of the muscle fibers through the wall, circumferential near the midwall and progressively more inclined with respect to the equatorial plane when moving toward either the epicardium or the endocardium.

2.2 The cardiac connective tissue organization

Myocytes and coronary blood vessels are embedded in a complex extracellular matrix which consists of collagen and elastin, mainly. Caulfield and Borg [4] first used the scanning electron microscope (SEM) to reveal the basic organization of this connective tissue network. Other studies on the connective tissue of mammalian heart muscle give the description of the extracellular structures and their arrangement relative to cardiac muscle cells [4, 22, 23] . They described the three following classes of connective tissue organization: (i) interconnections between myocytes, (ii) connections between myocytes and capillaries and, (iii) a collagen weave surrounding group of myocytes. When viewed by SEM, groups of myocytes can be seen to be encompassed by a rather prominent meshwork of fibrillard collagen, and short collagen struts (similar to those that attach adjacent myocytes to each other) attach the myocytes subjacent to this meshwork to it.

3 The mechanical model and its finite element formulation

3.1 Mechanical coupling between muscle fibers and connective tissue

Extrapolations from the muscle fiber arrangement to the myocardial stress are realistic when also taking account the effect of the connective tissue. We believe that a part of that connective tissue, surrounding group of myocytes, is responsible for the active tension developed in the perpendicular direction of the muscle fibers running on the tangential plane of the ventricular wall. Based on the previous SEM observations, we propose a connective tissue organization illustrated on figure 2. We assume that the myocytes are roughly cylindrical and that groups of myocytes are surrounded by inextensible collagen networks. So, during the contraction, the myocytes diameter increases and because the collagen network is inextensible, the adjacent muscle cells become closer. Thus the pseudo-active kinematic relation between the muscle fiber and cross-fiber extension ratios (noted λ_f and λ_{cf}, respectively) is $h(\lambda_f, \lambda_{cf}) = 0$ with:

$$h(\lambda_f, \lambda_{cf}) = 1 - \lambda_{cf} + (\pi - 2)(1 - \lambda_f^{-1/2})\frac{a}{D} \tag{1}$$

with $D = 4a + d$ where a is the initial myocyte radius and d is the distance between the two cells (Fig. 2).

3.2 Constitutive law for the active cardiac tissue under internal pseudo-active kinematic constraint

To be consistent with our mathematical formulation, the letter $\mathbf{\Phi}$ is used for the non elastic gradient tensor and the letter $\mathbf{F}$ is used for the elastic gradient tensor. The activation of the muscle fibers changes the properties of the material and at the same time contracts the muscle itself. To have a continuous elastic description during the activation of the tissue, we used an approach similar to the one proposed by Ohayon and Chadwick [20], Taber [26], Lin and Yin [16]. From its passive zero-stress state P, the free activation of the muscle fibers is modelised by the following two transformations (Fig.1): the first one (from state P to virtual state A_0) changes the material properties without changing the geometry, and the second one (from A_0 to A) contracts the muscle without changing the properties of the material. Thus, the former is not an elastic deformation and is described by the gradient tensor $\mathbf{\Phi}_{PA_0} = \mathbf{I}$ where $\mathbf{I}$ is the identity matrix. In that first transformation, only the strain energy function is modified using an activation function $\beta(t)$, where t is the cardiac cycle time. The second transformation is an elastic deformation caused only by the active tension delivered by the fibers and takes care of the internal kinematic constraint (Eq.(1)). This last transformation is described by the gradient tensor $\mathbf{F}_{A_0A}$. Thus the transformation from state P to state A is a non elastic transformation ($\mathbf{\Phi}_{PA} = \mathbf{\Phi}_{PA_0}\mathbf{F}_{A_0A}$), but can be treated mathematically as an elastic one because $\mathbf{\Phi}_{PA} = \mathbf{F}_{A_0A}$. Finally, external loads are applied to state A deforming the body through into C (Fig.1). The change of the material properties of the myocardium during the cardiac cycle is described by a time-dependent strain-energy function per unit volume of state P noted $W(\mathbf{E}_{PH}, t)$:

$$W(\mathbf{E}_{PH}) = -\frac{1}{2}\, p_H(I_3(\mathbf{E}_{PH}) - 1) + W^*(\mathbf{E}_{PH}) + \delta_{AH}\, \underset{active}{W_{pseudo}}(\mathbf{E}_{PH}) \tag{2}$$

with

$$W^*(\mathbf{E}_{PH}) = W_{pas}(\mathbf{E}_{PH}) + \beta(t)\, W^f_{act}(\mathbf{E}_{PH}) \tag{3}$$

where $\mathbf{E}_{PH}$ is the Green's strain tensor at an arbitrary state H calculated from the zero strain state P (the state H could be one of the states A_0, A or C shown in figure 1), p_H is the Lagrangian multiplier resulting of the incompressibility constraint $\det \mathbf{\Phi}_{PH} = 1$, $I_3(\mathbf{E}_{PH})$ is the determinant of the right Cauchy-Green strain tensor $\mathbf{C}_{PH}$ ($\mathbf{C}_{PH} = 2\mathbf{E}_{PH}+\mathbf{I}$), W_{pas} represents the contribution of the surrounding collagen matrix and of the passive fiber components, W^f_{act} arises from the active component of the embedded muscle fibers, and $\beta(t)$ is an activation function equal to zero at end-diastolic state and equal to one at end-systolic state ($0 \leq \beta(t) \leq 1$). The scalar δ_{AH} is equal to one if state H is the state A and zero if the two states H and A are distinct. The term $W^f_{act}(\mathbf{E}_{PH})$ gives the variation of the muscle fibers properties during the cardiac cycle. The pseudo-active strain energy function expressed in the last term of the right hand side of the Eq.(2) is introduced in order to satisfy the kinematic condition (Eq.(1)) and is given by:

$$W_{\substack{pseudo\\active}}(\mathbf{E}_{PH}) = -\frac{1}{2} q_H \, h(\mathbf{E}_{PH}) \tag{4}$$

The scalar q_H introduced in Eq.(4) serves as an additional indeterminate Lagrange multiplier which contributes to the pseudo-active stresses at state H in fiber and the cross-fiber directions, and $h(\mathbf{E}_{PH})$ is the function defined in Eq.(1), which may be rewritten as:

$$h(\mathbf{E}_{PH}) = 1 - I_6^{1/2} + (\pi - 2)\,(1 - I_4^{-1/4})\,\frac{a}{D} \tag{5}$$

where I_4 and I_6 are two strain invariants given by $I_4(\mathbf{E}_{PH}) = \mathbf{f}_P \cdot \mathbf{C}_{PH} \cdot \mathbf{f}_P$ and $I_6(\mathbf{E}_{PH}) = \mathbf{f}^{\perp}_P \cdot \mathbf{C}_{PH} \cdot \mathbf{f}^{\perp}_P$ in which the fiber and the perpendicular fiber directions are respectively characterized in state P by the unit vectors $\mathbf{f}_P$ and $\mathbf{f}^{\perp}_P$. In an arbitrary deformed state H, the direction of these two unit vectors are noted $\mathbf{f}_H$ and $\mathbf{f}'_H$ and are respectively defined by $\mathbf{f}_H = \mathbf{\Phi}_{PH} \cdot \mathbf{f}_P / \parallel \mathbf{\Phi}_{PH} \cdot \mathbf{f}_P \parallel$ and $\mathbf{f}'_H = \mathbf{\Phi}_{PH} \cdot \mathbf{f}^{\perp}_P / \parallel \mathbf{\Phi}_{PH} \cdot \mathbf{f}^{\perp}_P \parallel$. The tensor $\mathbf{C}_{PH}$ is the right Cauchy-Green strain tensor ($\mathbf{C}_{PH} = 2\mathbf{E}_{PH} + \mathbf{I} = \mathbf{\Phi}^T_{PH}\mathbf{\Phi}_{PH}$). The superscript 'T' is used for transpose matrix and $\| \cdot \|$ stands for the euclidian norm. Note that I_4 and I_6 are directly related respectively to the fiber and cross-fiber extension ratios (we have $I_4 = \lambda_f^2$ and $I_6 = \lambda_{cf}^2$). In our notations λ_f is related to the fiber direction $\mathbf{f}_H$ and λ_{cf} to the cross-fiber direction $\mathbf{f}'_H$ (Figure 2). We treat the myocardium as a homogeneous, incompressible, and hyperelastic material transversely isotropic with respect to the local muscle fiber direction. In this study, we modified the strain-energy function suggested by Lin and Yin [16] by substracting the beating term and introducing an activation function $\beta(t)$ which allows to describe continuously the phases of the cardiac cycle:

$$W_{pas}(\mathbf{E}_{PH}) = C^p_1(e^Q - 1) \tag{6}$$

$$\text{with} \qquad Q = C^p_2(I_1 - 3)^2 + C^p_3(I_1 - 3)(I_4 - 1) + C^p_4(I_4 - 1)^2 \tag{7}$$

$$\text{and} \qquad W^f_{act}(E_{PH}) = C^a_1(I_1 - 3)(I_4 - 1) + C^a_2(I_1 - 3)^2 + C^a_3(I_4 - 1)^2 + C^a_4(I_1 - 3) \tag{8}$$

where ($C^p_i, \quad i = 1, \cdots, 4$) and ($C^a_i, \quad i = 1, \cdots 4$) are material constants and I_1 is the first principal strain invariant given by $I_1(\mathbf{E}_{PH}) = tr\, \mathbf{C}_{PH}$.
To incorporate the active contraction, an active fiber stress $\beta\, T^{(0)}$ was applied in the deformed fiber direction. In our approach, the active loaded state C of the myocardial tissue is obtained in two steps. In the first step and at a given degree of activation β, we derived and quantified

the internal pseudo-active stresses by looking the free contraction configuration of the tissue (state A, Figure 1). Then, in a second step, we applied the loads on the active myocardial tissue under the internal pseudo-active stresses previously found.

Determination of the free contraction state A**-** During the cardiac cycle and at a given degree of activation β, the Cauchy stress tensor in state A (noted $\boldsymbol{\tau}_A$) is given by:

$$\boldsymbol{\tau}_A = -p_A\mathbf{I} + \boldsymbol{\Phi}_{PA}\frac{\partial W^*\left(\mathbf{E}_{PA}\right)}{\partial \mathbf{E}_{PA}}\boldsymbol{\Phi}_{PA}^T + \beta(t)T^{(0)}\mathbf{f}_A \otimes \mathbf{f}_A + \boldsymbol{\tau}_A^{\overset{pseudo}{active}} \tag{9}$$

$$\text{with} \qquad \boldsymbol{\tau}_A^{\overset{pseudo}{active}} = \boldsymbol{\Phi}_{PA}\frac{\partial W_{\underset{active}{pseudo}}\left(\mathbf{E}_{PA}\right)}{\partial \mathbf{E}_{PA}}\boldsymbol{\Phi}_{PA}^T \tag{10}$$

where the symbol $\otimes$ denotes the tensor product. The postulated mechanical coupling law (Eq.(5)) induces, during the contraction, a pseudo-active stress tensor (noted $\boldsymbol{\tau}_A^{\overset{pseudo}{active}}$) with stress components in the fiber and cross-fiber direction:

$$\boldsymbol{\tau}_A^{\overset{pseudo}{active}} = T_A^f\,\mathbf{f}_A \otimes \mathbf{f}_A + T_A^{cf}\,\mathbf{f}'_A \otimes \mathbf{f}'_A \tag{11}$$

These two stress tensor components T_A^f and T_A^{cf} are activation-dependent and behave as some internal tensions in the fiber and cross-fiber directions of unit vectors $\mathbf{f}_A$ and $\mathbf{f}'_A$, respectively. These pseudo-active tensions are defined by:

$$T_A^f = 2\,\frac{\partial W_{\underset{active}{pseudo}}\left(\mathbf{E}_{PA}\right)}{\partial I_4\left(\mathbf{E}_{PA}\right)}\;\|\;\boldsymbol{\Phi}_{PA}\cdot\mathbf{f}_P\;\|^2 \quad \text{and} \quad T_A^{cf} = 2\,\frac{\partial W_{\underset{active}{pseudo}}\left(\mathbf{E}_{PA}\right)}{\partial I_6\left(\mathbf{E}_{PA}\right)}\;\|\;\boldsymbol{\Phi}_{PA}\cdot\mathbf{f}_P^{\perp}\;\|^2 \tag{12}$$

Determination of the physiological active loaded state C**-** As we have modelised the active fiber tension $\beta(t)T^{(0)}$, we incorporate these previously found internal pseudo-active tensions T_A^f and T_A^{cf} in the expression of the stress tensor at loaded state C. Therefore, at a given time (or activation β) of the cardiac cycle, the Cauchy stress tensor in the physiological state C (noted $\boldsymbol{\tau}_C$) is written as:

$$\boldsymbol{\tau}_C = -p_C\mathbf{I} + \boldsymbol{\Phi}_{PC}\frac{\partial W^*\left(\mathbf{E}_{PC}\right)}{\partial \mathbf{E}_{PC}}\boldsymbol{\Phi}_{PC}^T + \left(\beta(t)T^{(0)} + T_A^f\right)\,\mathbf{f}_C \otimes \mathbf{f}_C + T_A^{cf}\,\mathbf{f}'_C \otimes \mathbf{f}'_C \tag{13}$$

The suggested constitutive law for the active myocardium (Eqs.(2)-(13)) makes it possible to simulate the left ventricle behavior during the whole cardiac cycle. Thus, in this law: (i) the anisotropic behavior is incorporated in the expression of the passive, active and pseudo-active strain energy functions by the terms I_4 and I_6, (ii) the contraction is accounted for by an active stress $\beta\,T^{(0)}$ in the fiber direction, (iii) the change of properties is expressed by the active strain energy term $\beta(t)\,W_{act}^f$, and (iv) the coupling effect between the collagen network and the muscular fibers is accounted for by the two internal pseudo-active tensions T_A^f and T_A^{cf} in the fiber and cross fiber directions $\mathbf{f}_C$ and $\mathbf{f}'_C$, respectively.

3.3 Variational formulation

The undeformed body state P contains a volume V bounded by a closed surface $\mathcal{A}$, and the arbitrary deformed body state is, as before, noted H. The corresponding position vectors, in cartesian base unit vectors, are $\mathbf{R} = Y^R\mathbf{e}_R$ and $\mathbf{r} = y^r\mathbf{e}_r$, respectively. However, we

write the equations with suitable curvilinear systems of world coordinates noted Θ^{A} in the reference configuration (state P) and θ^α in the deformed configuration (state H): see Figure 3. In this paper we use the following conventional notations: (i) capital letters are used for coordinates and indices of tensor components associated to state P, and lower case letters are related to state C, and (ii) $\mathbf{G}$ and $\mathbf{g}$ are the base vectors in states P and C, respectively, for which parenthetical superscript indicates the associated coordinate system (see table 1, for example $\mathbf{G}_I^{(x)} = \partial\mathbf{R}/\partial X^I = \mathbf{R}_{,I}^{(x)}$ and $\mathbf{g}_i^{(x)} = \partial\mathbf{r}/\partial x^i = \mathbf{r}_{,i}^{(x)}$).
The Lagrangian formulation of the virtual works principle is given by

$$\int_V P_H^{IJ}\Phi_{\cdot J}^{\cdot\alpha}\nabla_I(\delta u_\alpha)\,dV = \int_V \rho(b^\alpha - \gamma^\alpha)\delta u_\alpha\,dV + (1-\delta_{AH})\int_{A_2}\mathbf{s}.\boldsymbol{\delta}\mathbf{u}\,dA \tag{14}$$

where P_H^{IJ} are the components of the second Piola-Kirchhoff stress tensor at state H, defined by $\mathbf{P}_H = \boldsymbol{\Phi}_{PH}^{-1}\,.\,\boldsymbol{\tau}_H\,.\,(\boldsymbol{\Phi}_{PH}^{-1})^T$, referred to the base tensor $\mathbf{G}_I^{(x)}\otimes\mathbf{G}_J^{(x)}$, $\Phi_{\cdot I}^{\cdot\alpha} = \partial\theta^\alpha/\partial X^I$ are the components of the gradient tensor $\boldsymbol{\Phi}_{PH}$ in the base tensor $\mathbf{g}_\alpha^{(\theta)}\otimes\mathbf{G}^{(x)I}$, $\boldsymbol{\delta}\mathbf{u} = \delta u_\alpha\mathbf{g}^{(\theta)\alpha}$ is an arbitrary admissible displacement vector, $\nabla_I(\delta u_\alpha) = \partial\delta u_\alpha/\partial X^I - \mathbf{g}_{\alpha,I}^{(\theta)}\cdot\mathbf{g}^{(\theta)\beta}\delta u_\beta$ are the components of the covariant differentiation vector $\boldsymbol{\delta}\mathbf{u}$ in the base vectors $\mathbf{g}^{(\theta)\alpha}$ (i.e. $\nabla_I(\delta u) = \nabla_I(\delta u_\alpha)\mathbf{g}^{(\theta)\alpha}$). The previous differentiation is done with respect to the locally orthonormal body coordinates ($X^I,\ I=1,2,3$) which coincide with the local muscle fiber direction in state P. The material density in the undeformed body state P is ρ, $\mathbf{b} = b^\alpha\mathbf{g}_\alpha^{(\theta)}$ is the body force vector per unit mass, $\boldsymbol{\gamma} = \gamma^\alpha\mathbf{g}_\alpha^{(\theta)}$ is the acceleration vector, $\mathbf{s}$ is the surface traction per unit area of $\mathcal{A}$, and A_2 is the part of $\mathcal{A}$ not subject to displacement boundary conditions.
The Lagrangian formulation for incompressibility is givenby

$$\int_V \left(\det g_{IJ}^{(x)} - 1\right)\,p^*\,dV = 0 \tag{15}$$

where the metric tensor $g_{IJ}^{(x)}$ is the metric tensor and p^* is an arbitrary admissible pressure. Lastly the Lagrangian formulation for the additional pseudo-active kinematic constraint is given by

$$\delta_{AH}\int_V h(I_4, I_6)\,q^*\,dV = 0 \tag{16}$$

for all admissible q^*. Eqs.(14)-(15) -(16) represent the variational formulation of a system of nonlinear partial differential equations.

3.4 Finite element approximation

Through this paper we use a three dimensional finite element with Lagrange trilinear interpolation for the displacements and uniform Lagrangian multipliers to compute an approximate solution of Eqs.(14)-(15)-(16)) on a rectangular mesh, where we neglect the acceleration and body forces ($\mathbf{b}=0$, $\boldsymbol{\gamma}=0$). This element is commonly used and is relevant for the finite element approximation of this type of problem where kinematics constraints must be satisfied [8].
Let (ξ_K) the Lagrangian normalized finite element coordinates (Figure 3), the deformed geometric coordinates θ^α in element e are interpolated as

$$\theta^{\alpha} = \sum_{n(e)=1}^{8} \psi_{n(e)}(\xi_1, \xi_2, \xi_3)\, \theta^{\alpha}_{n(e)} \tag{17}$$

where $\psi_{n(e)}$ is the base function associated with the local node $n(e)$ and $\theta^{\alpha}_{n(e)}$ is the α-coordinate of the local node n of element e.

Let $\Omega_{\Delta}^{n(e)}$ be the connectivity matrix defined by

$$\Omega_{\Delta}^{n(e)} = \begin{cases} 1 & \text{if} \quad \Delta(n(e), e) = \Delta \\ 0 & \text{otherwise} \end{cases} \tag{18}$$

where $\Delta(p, e)$ is the global node corresponding with the local node p of the element e. Since we use one single cartesian coordinate system ($(\Theta^{\mathrm{A}}) = (X^I) = (Y^R)$ and $(\theta^{\alpha}) = (x^i) = (y^r)$), we denote the nodal displacements θ^{α}_{Δ} by y^{α}_{Δ}. Then the FE approximation of Eqs.(14)-(15)-(16) is

$$\sum_{e} \sum_{n(e)=1}^{8} \Omega_{\Delta}^{n(e)} \int_{V_e} P_H^{IJ}\, \Phi_J^{\cdot\alpha}\, \nabla_I(\psi_{n(e)})\, dV \;=\; (1 - \delta_{AH}) \sum_{e} \sum_{n(e)=1}^{8} \Omega_{\Delta}^{n(e)} \int_{A_{2_e}} s^{\alpha}\, \psi_{n(e)}\, dA \tag{19}$$

$$\int_{V_e} \left(\det g^{(x)}_{IJ} - 1 \right) dV \;=\; 0 \tag{20}$$

$$\delta_{AH} \int_{V_e} h(I_4, I_6)\, dV = 0 \tag{21}$$

with $\Delta = 1, \cdots, \Delta_{max}$, $\alpha = 1, 2, 3$, where A_{2_e} is the part of A_e (boundary of element e) non subject to displacement conditions.

3.5 Finite element solution method

We proceed in two steps. The first one consists in the determination of the pseudo- active stresses T_A^f and T_A^{cf} as functions of the activation parameter $\beta \in [0, 1]$ by looking for the state A ($\delta_{AH} = 1$). We solve the system (19)-(20)-(21) with zero right hand side for (19) (free active contraction) and P_A^{IJ} given by

$$\begin{aligned} P_A^{IJ} \;=\; & -p_A\, g^{(x)IJ} + 2G^{(x)IJ}\, W_1^* + (2\, W_4^* - q_A\, h_4)\, \delta^{1I}\delta^{1J} \\ & + \beta(t)\, T^{(0)} \frac{\delta^{1I}\delta^{1J}}{\| \mathbf{g}_1^{(x)} \|^2} - q_A\, h_6\, \delta^{2I}\delta^{2J} \end{aligned} \tag{22}$$

$$\text{where} \qquad W_i^* \;=\; \frac{\partial W^*}{\partial I_i} = \frac{\partial W_{pas}}{\partial I_i} + \beta_W(t)\, \frac{\partial W^f_{act}}{\partial I_i} + \delta_{AH}\, \frac{\partial W_{\substack{pseudo \\ active}}}{\partial I_i} \quad i = 1,\, 4 \tag{23}$$

$$\text{and} \qquad h_i \;=\; \frac{\partial h(I_4, I_6)}{\partial I_i} \quad i = 4,\, 6 \tag{24}$$

The unknowns of this nonlinear system of equations are $(y^{\alpha}_{\Delta}, p_A(e), q_A(e))$ with $\alpha = 1, 2, 3$, $\Delta = 1, \cdots, \Delta_{max}$ and $e = 1, \ldots, e_{max}$ where e_{max} is the total number of elements involved

in the mesh. We derive T_A^f and T_A^{cf} for a given β according to Eq.(12). Then in a next step we can compute any physiological active loaded state C solving the system (19)-(20) with $\delta_{AH} = 0$ and P_C^{IJ} given by

$$\begin{aligned} P_C^{IJ} &= -p_C\, g^{(x)IJ} + 2G^{(x)IJ}\, W_1^* + 2\, W_4^*\, \delta^{1I}\delta^{1J} \\ &\quad +(\beta(t)\, T^{(0)} + T_A^f)\, \frac{\delta^{1I}\delta^{1J}}{\| \mathbf{g}_1^{(x)} \|^2} + T_A^{cf}\, \frac{\delta^{2I}\delta^{2J}}{\| \mathbf{g}_2^{(x)} \|^2} \end{aligned} \tag{25}$$

To solve the sytem in both cases we use the Powell method [21]. This method is a quasi Newton method which consists in: (i) computing the jacobian matrix of an iterate by forward differences (with step h=10^{-8}) and (ii) searching the new iterate on a steepest descent line of the jacobian by the so called "dogleg method" [28]. For this sake, we use the package MINPACK [18]. Moreover, one can observe that in equation (19)-(20), the nonlinear functions involve 3D and 2D integrals over a rectangular domain. Thus we use adaptive gaussian quadrature method to evaluate with a very good precision (up to 10^{-12}) these integrals. For this purpose, we use the package DCUHRE [2]. Our numerical code named SAMUEL (for "Solid Active MUscle ELement") is implemented in Fortran 77 on Personal Computers under LinuX operating system.

4 Results

We simulated the loading of a thin sample of myocardium ($1.0 \times 1.0 \times 0.1$ cm^3) in which the fibers are uniformly oriented in one direction (Y_1). We compared the exact solution to the numerical one obtained for the cases of a free contraction, uniaxial and equibiaxial extension of a rectangular mesh. These comparisons show an error less than 10^{-12} in the L^2 norm. In the case of a free active contraction (Fig.4) we observe an important effect of the kinematic constraint in the cross-fiber directions cf and cf': contraction in the direction cf and a thickening effect in the direction cf'. The effect of the pseudo- active stresses T_A^f and T_A^{cf} can be observed in the cases of active or passive uniaxial (Fig.5) and equibiaxial (Fig.6) extension tests. We show in tables 2 and 3 the effect of the geometric parameters a, d (see Fig.2) and of the maximal active tension $T^{(0)}$ on the internal pseudo-active tensions T_A^f, T_A^{cf} and on the ratio between the cross fiber (cf) Cauchy stress σ_{22} and the fiber (f) Cauchy stress σ_{11}.

References

[1] N. R. Alpert. *Cardiac hypertrophy.* Academic Press, New-York, 1971.

[2] J. Berntsen, T. O. Espelid, and A. Genz. Algorithm 698: DCUHRE: An adaptive multidimensional integration routine for a vector of integrals. *ACM Trans. Math. Softw.*, 17(4):452–456, 1991.

[3] P.H.M. Bovendeerd, T. Arts, J.M. Huyghe, D.H. van Campen, and R.S. Reneman. Dependance of local left ventricular wall mechanics on myocardial fiber orientation: a model study. *J. Biomech.*, 25:1129–1140, 1992.

[4] J. B. Caulfield and T. .K Borg. The collagen network of the heart. *Lab. Invest.*, 40(3):364–372, 1979.

[5] R. S. Chadwick, A. Tedgui, J.B Michel, J. Ohayon, and B. I Levy. Phasic regional myocardial inflow and outflow : comparison of theory and experiments. *Am. J. Physiol.*, 258:H1687–1698, 1990.

[6] K.D. Costa, P.J. Hunter, J.S. Wayne, L.K. Waldman, J.M. Guccione, and A.D. McCulloch. A three-dimensional finite element method for large elastic deformations of ventricular myocardium: Part I - Cylindrical and spherical polar coordinates. *ASME J. Biomech. Eng*, 118:452–463, 1996.

[7] K.D. Costa, P.J. Hunter, J.S. Wayne, L.K. Waldman, J.M. Guccione, and A.D. McCulloch. A three-dimensional finite element method for large elastic deformations of ventricular myocardium: Part II - Prolate spheroidal coordinates. *ASME J. Biomech. Eng*, 118:464–470, 1996.

[8] R. Glowinsky and P. Le Tallec. *Augmented lagrangian and operator-splitting methods in nonlinear mechanics*. SIAM, Philadelphia, PA, 1989.

[9] W. Grossman. Cardiac hypertrophy : useful adaptation or pathological process ? *Am. J. of Medicine*, 69:576–584, 1980.

[10] J.M. Guccione and A.D. McCulloch. Finite element modeling of ventricular mechanics. In L. Glass, P.J. Hunter, and A.D. McCulloch, editors, *Theory of heart: biomechanics, biophysics and nonlinear dynamics of cardiac function*, pages 121–144, New York, 1991. Springer Verlag.

[11] A. Horowitz, I. Sheinman, and Y. Lanir. Nonlinear incompressible finite element for simulating loading of cardiac tissue. *ASME J. Biomech. Eng.*, 110:62–68, 1988.

[12] P.J. Hunter, A.D. McCulloch, P.M.F. Nielsen, and B.H. Smaill. A finite element model of passive ventricular mechanics. In R.L. Spilker and B.R. Simon, editors, *Computational methods in bioengineerig*, pages 387–397, Chicago, 1988. ASME.

[13] J.M. Huyghe, D.H. van Campen, T. Arts, and R.M. Heethaar. A two-phase finite element model of the diastolic left ventricle. *J. Biomech.*, 24:527–538, 1991.

[14] I.J. LeGrice IJ, Y. Takayama, and J.W.J. Covell. Transverse shear along myocardial cleavage planes provides a mechanism for normal systolic wall thickening. *Circ. Res.*, 77:182–193, 1995.

[15] K.-M. Jan. Distribution of myocardial stress and its influence of coronary blood flow. *J. Biomech.*, 18:815–820, 1985.

[16] D.H.S. Lin and F.C.P. Yin. A multiaxial constitutive law for mammalian left ventricular myocardium in steady-state barium contracture or tetanus. *J. Biomech. Eng.*, 120:504–517, 1998.

[17] A.D. McCulloch, L.K. Waldman, J. Rogers, and J. Guccione. Large scale finite element analysis of the beating heart. *Crit. Rev. Biomed. Eng.*, 20:427–449, 1992.

[18] J.J. Morge, B. S. Garbow, and K. E. Hillstrom. User Guide for MINPACK-1. Technical Report ANL–80–74, Argonne National Laboratory, March 1980.

[19] J. Ohayon, H. Cai, P.S. Jouk, Y. Usson, and A. Azancot. A model of the structural and functional development of the normal human fetal left ventricle based on a global growth law. *Comp. Meth. Biomech. & Biomed. Engin.*, 5(2):113–126, 2002.

[20] J. Ohayon and R.S. Chadwick. Effects of collagen microstructure on the mechanics of the left ventricle. *Biophys. J.*, 54:1077–1088, 1988.

[21] M.J.D. Powell. A hybrid method for nonlinear equations. In P. Rabinowitz, editor, *Numerical methods for nonlinear algebraic equations*, pages 87–114, New York, 1970. Gordon and Breach.

[22] T. F. Robinson, L. Cohen-Gould, and S. M. Factor. Skeletal framework of mammalian heart muscle. arrangement of inter- and pericellular connective tissue structures. *Lab. Invest.*, 49:482–498, 1983.

[23] T. F. Robinson, S. M. Factor, J. M. Capasso, B. A. Wittenburg, O. O. Blumenfeld, and S. Seifter. Morphology, composition, and function of struts between cardiac myocytes of rat and hamster. *Cell Tissue Res.*, pages 249–247, 1987.

[24] S.J. Sarnoff, E. Braunwald, G.H. Jr. Welch, R. B. Case, W. N. Stainsby, and R. Macruz. Hemodynamic determinants of oxygen consumption of the heart with special reference to the tension-time index. *Am. J. Phsysiol.*, 192:148–156, 1958.

[25] D.D. Streeter. Gross morphology and fiber geometry of the heart. In R. M. Berne et al., editor, *Handbook of physiology*, volume 1, pages 61–112, Bethesda MD, 1979. American Physiological Society.

[26] L.A. Taber. On a nonlinear theory for muscle shells: Part II- Application to the beating left ventricle. *J. Biomech. Eng.*, 113:63–71, 1991.

[27] L.A. Taber. Biomechanics of growth, remodeling, and morphogenesis. *Appl. Mech. Rev*, 48(8):487–545, 1995.

[28] J. Zhang and C. Xu. A class of indefinite dogleg path mehods for unconstrained minimization. *SIAM J. Optim.*, 9(3):646–667, 1999.

5 Figures

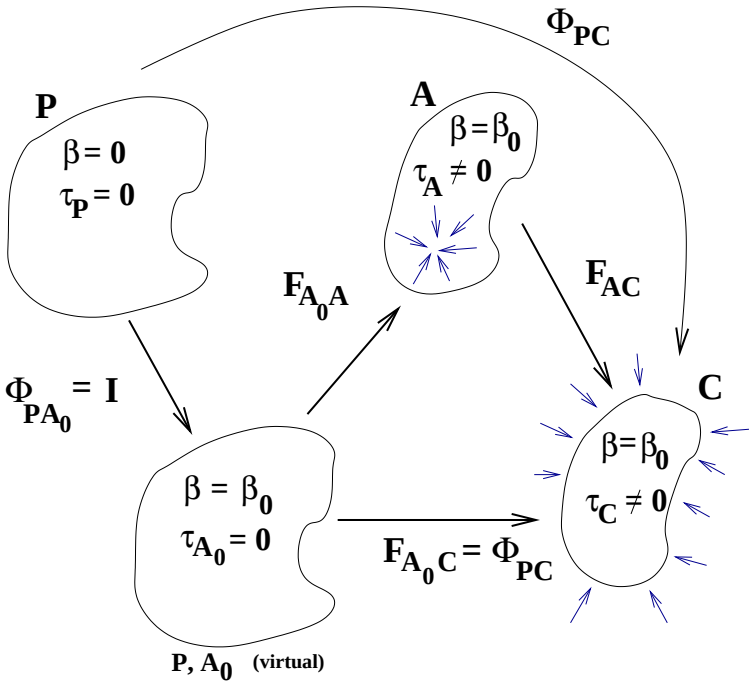

Figure 1: Description of the active rheology approach (see text for more details).

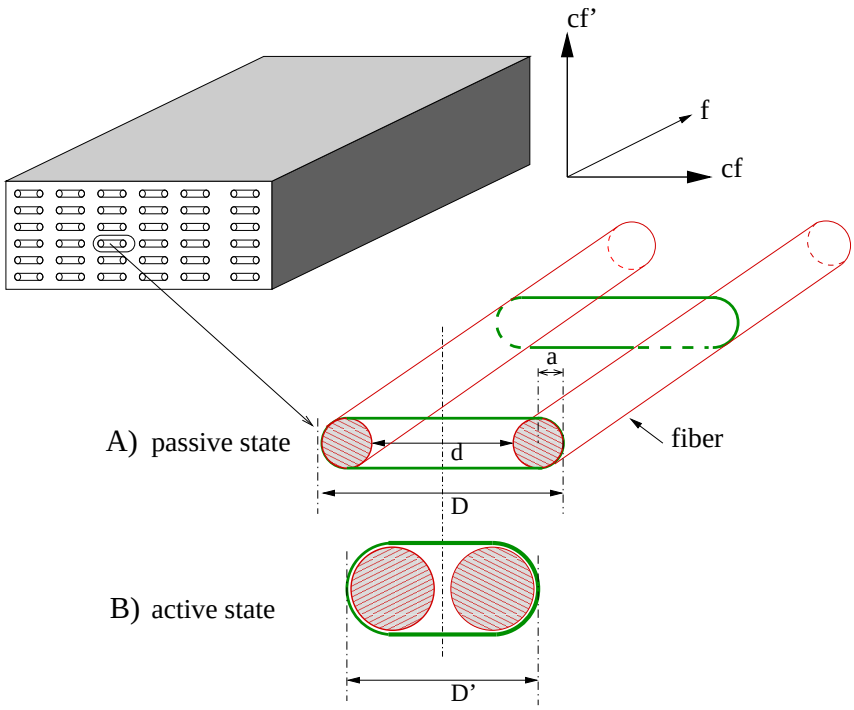

Figure 2: Schematic illustration of the internal pseudo-active kinematic constraint induced by the collagen network surrounding the myocytes. A) Before contraction. B) After or during contraction.

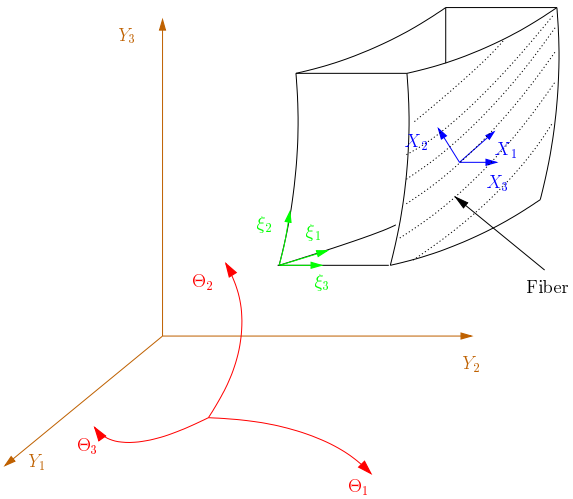

Figure 3: Coordinate systems (adapted from Costa et al. [6, 7]).

	State	Indices	Coord.	Covariant base vectors	Contravariant base vectors	Metric tensors	
(I)	P	R, S	Y^R	$\mathbf{e}_R$	$\mathbf{e}_R$	δ_{RS}	δ^{RS}
	H	r, s	y^r	$\mathbf{e}_r$	$\mathbf{e}_r$	δ_{rs}	δ^{rs}
(II)	P	A, B	Θ^A	$\mathbf{G}_A^{(\theta)} = \dfrac{\partial \mathbf{R}}{\partial \Theta^A}$	$\mathbf{G}^{(\theta)A}$	$G_{AB}^{(\theta)}$	$G^{(\theta)AB}$
	H	α, β	θ^α	$\mathbf{g}_\alpha^{(\theta)} = \dfrac{\partial \mathbf{r}}{\partial \theta^\alpha}$	$\mathbf{g}^{(\theta)\alpha}$	$g_{\alpha\beta}^{(\theta)}$	$g^{(\theta)\alpha\beta}$
(III)	P	K, L	ξ^K	$\mathbf{G}_K^{(\xi)} = \dfrac{\partial \mathbf{R}}{\partial \xi^K}$	$\mathbf{G}^{(\xi)K}$	$G_{KL}^{(\xi)}$	$G^{(\xi)KL}$
(IV)	P	I, J	X^I	$\mathbf{G}_I^{(x)} = \dfrac{\partial \mathbf{R}}{\partial X^I}$	$\mathbf{G}^{(x)I}$	$G_{IJ}^{(x)} = \delta_{IJ}$	$G^{(x)IJ} = \delta^{IJ}$
	H			$\mathbf{g}_I^{(x)} = \dfrac{\partial \mathbf{r}}{\partial X^I}$	$\mathbf{g}^{(x)I}$	$g_{IJ}^{(x)}$	$g^{(x)IJ}$
	P	i, j, k, l	x^i	$\mathbf{G}_i^{(x)} = \dfrac{\partial \mathbf{R}}{\partial x^i}$	$\mathbf{G}^{(x)i}$	$G_{ij}^{(x)}$	$G^{(x)ij}$
	H			$\mathbf{g}_i^{(x)} = \dfrac{\partial \mathbf{r}}{\partial x^i}$	$\mathbf{g}^{(x)i}$	$g_{ij}^{(x)} = \delta_{ij}$	$g^{(x)ij} = \delta^{ij}$

Table 1: Notations for the coordinate systems used to formulate finite element method (adapted from Costa et al. [6, 7]). (I) Rectangular cartesian reference coordinates, (II) Curvilinear world coordinates, (III) Normalized finite element coordinate, (IV) Locally orthonormal body/fiber coordinates. H stands for A or C

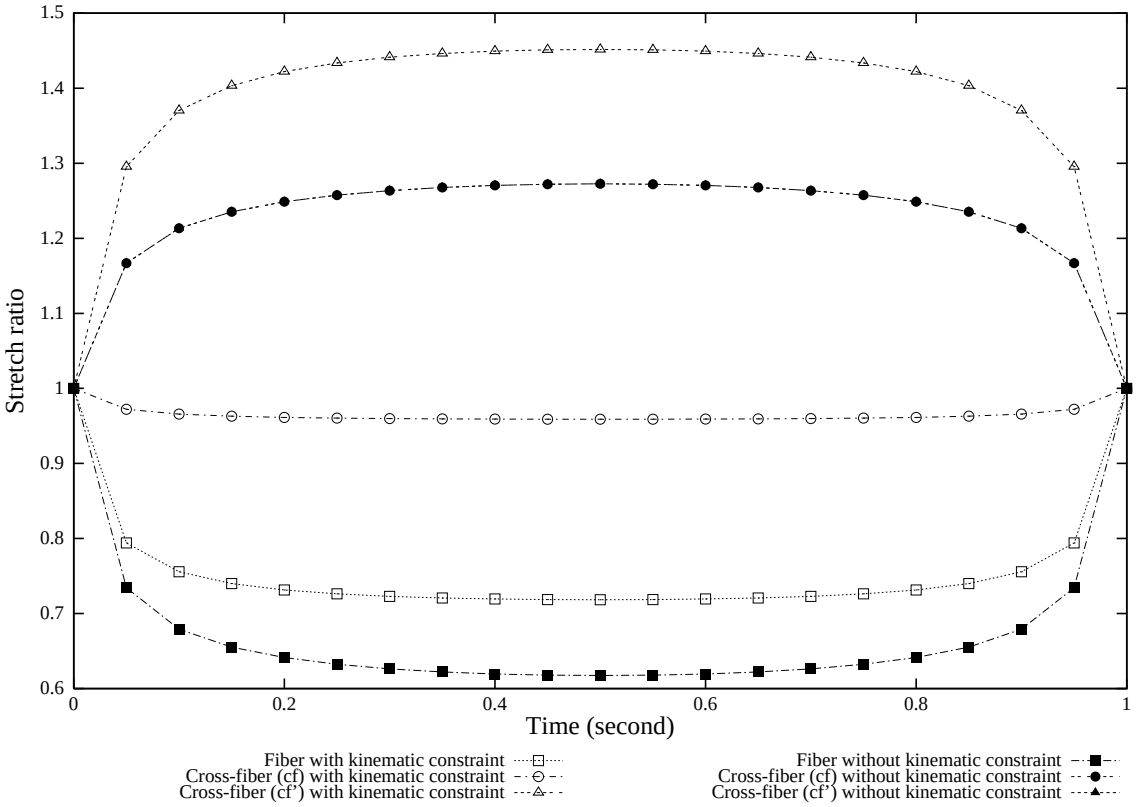

Figure 4: Free contraction test: effect of the pseudo-active kinematic constraint. Notice that without kinematic constraint, cross-fiber (cf) and (cf') stretch ratio curves are the same

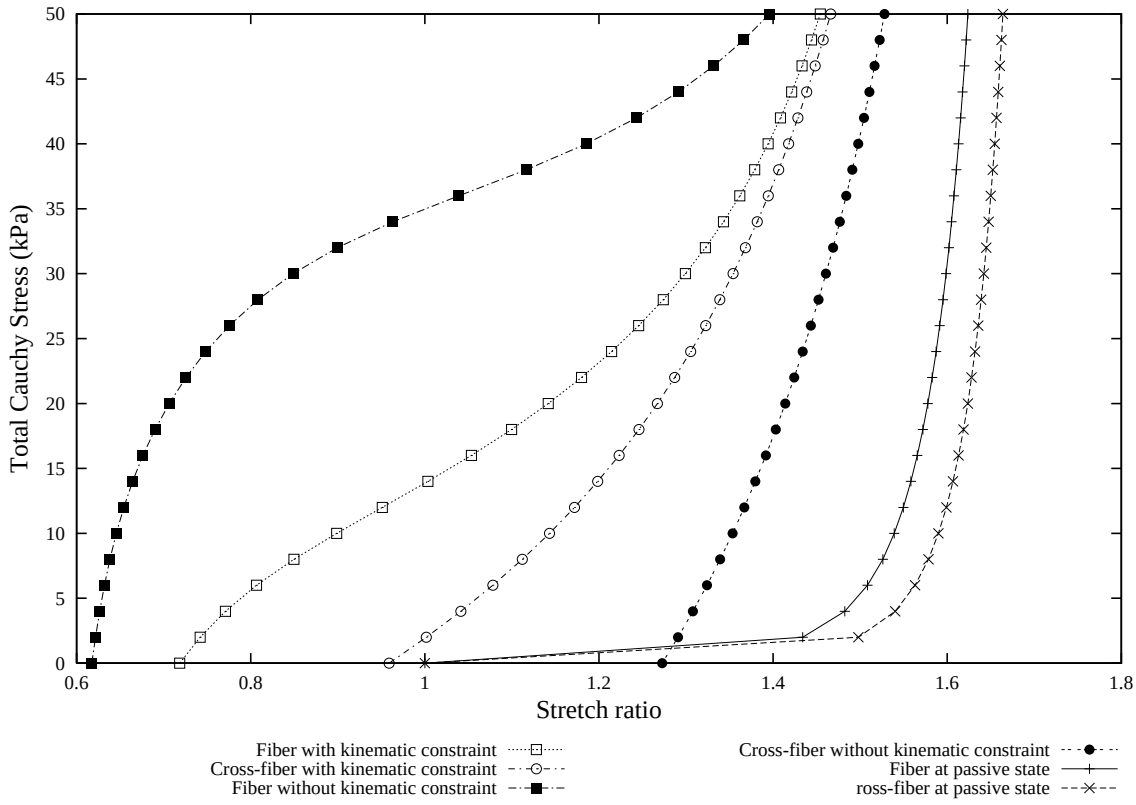

Figure 5: Active and passive uniaxial extension tests: effect of the pseudo-active kinematic constraint

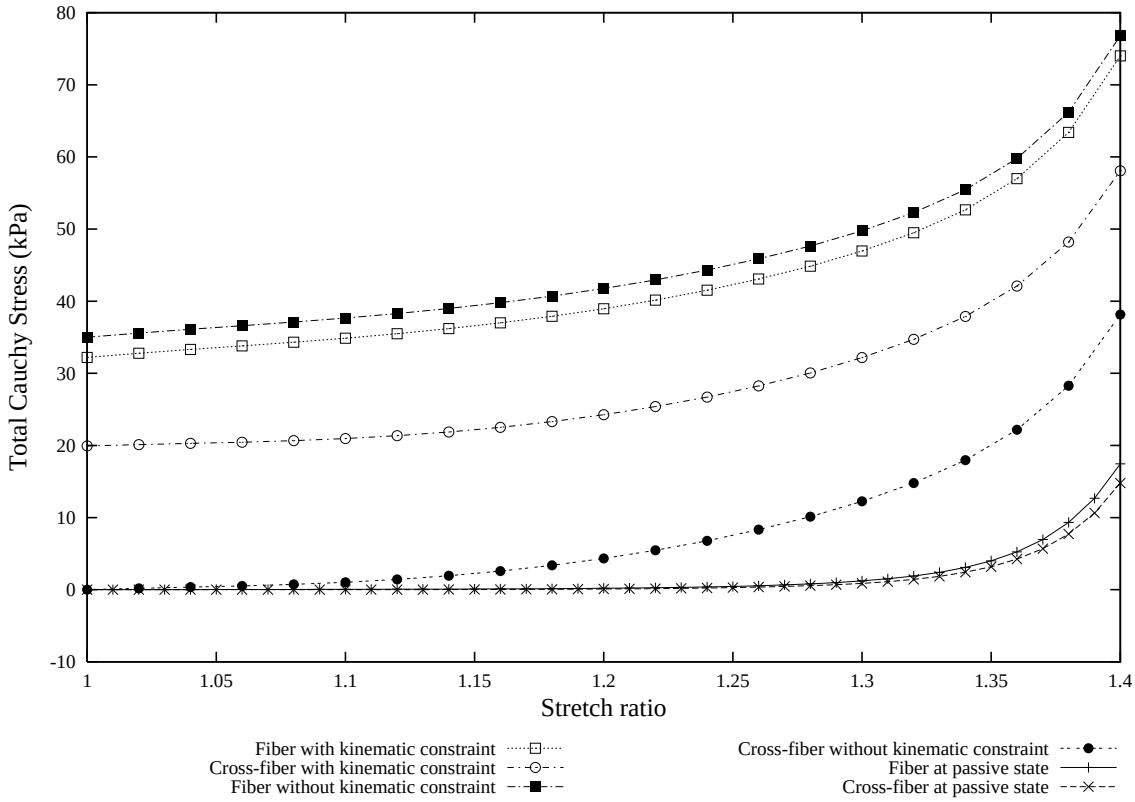

Figure 6: Active and passive equibiaxial extension tests: effect of the pseudo-active kinematic constraint

a/d \ $T_0\ (KPa)$		5	15	25	35	45
0.10	T_A^f/T_0 (%)	-1.98	-3.11	-3.66	-3.97	-4.15
	T_A^{cf}/T_0 (%)	32.23	47.42	53.82	57.13	59.01
0.15	T_A^f/T_0 (%)	-3.03	-4.72	-5.52	-5.98	-6.63
	T_A^{cf}/T_0 (%)	32.91	47.73	53.90	57.11	58.92
0.20	T_A^f/T_0 (%)	-4.13	-6.34	-7.39	-8.00	-8.36
	T_A^{cf}/T_0 (%)	33.50	47.91	53.85	56.93	58.69

Table 2: Free contraction at $\beta = 1$. Effect of the geometric parameters a, d (see Fig.2) and of the maximal active tension $T^{(0)}$ on the internal pseudo-active tensions T_A^f and T_A^{cf}

a/d \ $T_0\ (KPa)$		5	15	25	35	45
0.10	σ_{22}/σ_{11} (%)	50.92	53.73	57.65	60.25	61.90
	$\sigma_{22}\ (KPa)$	5.94	11.44	17.78	24.32	30.88
0.15	σ_{22}/σ_{11} (%)	51.44	54.56	58.60	61.30	63.01
	$\sigma_{22}\ (KPa)$	5.97	11.48	17.80	24.31	30.84
0.20	σ_{22}/σ_{11} (%)	51.94	55.33	59.47	62.25	64.04
	$\sigma_{22}\ (KPa)$	6.00	11.51	17.79	24.25	30.73
No kinematic constraint	σ_{22}/σ_{11} (%)	36.78	19.88	13.62	10.36	8.36
	$\sigma_{22}\ (KPa)$	4.32	4.32	4.32	4.32	4.32

Table 3: Equibiaxial active loading at $\lambda_1 = \lambda_2 = 1.2$. Effect of the geometric parameters a, d (see Fig.2) and of the maximal active tension $T^{(0)}$ on the ratio between the cross fiber Cauchy stress σ_{22} and the fiber Cauchy stress σ_{11}